MATEC Web of Conferences **14**, 09003 (2014)
DOI: 10.1051/matecconf/20141409003

Evolution of secondary phases in alloy ATI 718Plus® during processing

Ana Casanova[1,a], Nuria Martín-Piris[2], Mark Hardy[3], and Catherine Rae[1]

[1] Department of Materials Science and Metallurgy, University of Cambridge, Pembroke Street, Cambridge CB2 3QZ, UK
[2] Escuela de Ingeniería Aeronáutica y del Espacio, Plaza del Cardenal Cisneros 3, 28040 Madrid, Spain
[3] Rolls-Royce plc, PO Box 31, Derby DE24 8BJ, UK

Abstract. ATI 718Plus® is a polycrystalline Ni-base superalloy for aero-engine disc applications, which relies on the precipitation of η-phase (Ni_6Nb[Al,Ti], $D0_{24}$) at grain boundaries for resistance to intergranular failure and grain size control. The nucleation and evolution of the η particles have been examined throughout the manufacturing process. During hot working below the η solvus, existing precipitates lose their orientation relationship with the matrix and become aligned with the forging flow. During heat treatment, a dual morphology develops by the uniform growth of those incoherent precipitates into coarse plates, together with the new nucleation of thin lamellae from selected grain boundaries. The balance between the two morphologies in the final component can be achieved by controlling precipitation and dissolution processes during forging.

1. Introduction

ATI 718Plus® (718Plus) is a polycrystalline Ni-base superalloy designed for use in static and rotating aero-engine components [1,2]. It has an improved temperature capability over Inconel 718, combined with similarly good mechanical properties and processability. For these reasons, 718Plus is a promising candidate to replace other more expensive γ'-strengthened alloys such as Waspaloy or Udimet 720Li in applications where the service temperature does not exceed 675 °C [3].

The tensile and stress rupture properties of 718Plus have been extensively studied, as the alloy was first optimised for static applications [4–6]. However, its use in rotating components demands a fine balance between strength and resistance to fatigue crack initiation vs damage tolerance and creep resistance. A good understanding of the microstructure development during the varied operations involved in the production of disc rotors is essential to design a processing route leading to optimum mechanical properties.

2. Background

2.1. Grain Boundary Precipitation in 718Plus

Unlike alloy 718, which is strengthened by the precipitation of the metastable γ''-phase (Ni_3Nb, $D0_{22}$, tetragonal), the main hardening phase in 718Plus is γ' (Ni_3[Al,Nb,Ti], $L1_2$, cubic), which provides a higher thermal stability [6–9]. In order to strengthen the grain boundaries, a second phase with a plate-like morphology can be precipitated through adequate heat-treatment.

The nature of the grain boundary precipitates has been a subject of recent debate. They were initially identified as δ-phase (Ni_3Nb, $D0_a$, orthorhombic) as in alloy 718 [6,10,11]. While some early reports by Xie *et al.* indicated the presence of a hexagonal phase in 718Plus [12–14], this possibility remained largely unexplored. Recently Pickering *et al.* clarified the issue and demonstrated that grain boundary particles in 718Plus are principally composed of η phase (Ni_6Nb[Al,Ti], $D0_{24}$, hexagonal) interleaved with layers of δ [15].

It has been suggested that this configuration serves to accommodate local compositional variations, and that the ratio between the two phases could depend on the thermo-mechanical history of the material [15,16]. However, η appears to be the main constituent in the majority of precipitates, while the δ layers, sometimes only a few atomic layers thick, can only be detected using high-resolution techniques. Within the scope of this study only η-phase could be detected, and the precipitates will be referred to as η particles.

2.2. η structure in a rotating disc component

The effect of the η-phase on the mechanical properties of alloy 718Plus has received a good deal of attention, and it appears to depend strongly on the volume fraction, morphology and location of the precipitates [5,6,17,18]. A small amount of rod-shaped η particles, homogeneously distributed over most grain boundaries, is recommended to prevent notch sensitivity at high temperature and improve resistance to intergranular crack propagation [19]. In addition, the pinning effect of the grain boundary precipitates leads to a better control of the grain structure during hot working operations (when these take place below the relevant solvus temperature), essential to meet

[a] Corresponding author: ac773@cam.ac.uk

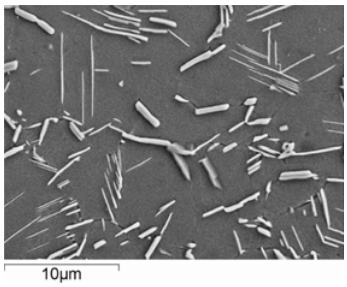

Figure 1. Secondary electron image of an electro-etched sample showing the dual η-phase morphology in a fully heat-treated disc.

the grain size target of ASTM 10–14 usually preferred in disc components for static strength and resistance to fatigue crack initiation [20].

The manufacturing of a superalloy disc rotor typically involves hot working a wrought billet in several steps, so as to develop the required geometry and refine the microstructure. Then, the strengthening and second-phase precipitate populations are optimised by heat treatment. Figure 1 shows the final microstructure of a 718Plus component after sub-solvus forging and standard heat treatment. A dual population of η precipitates is observed, in the form of blocky particles and cascades of thin lamellae.

In this study, 718Plus material was investigated at various stages during the manufacturing of a disc rotor, from the as-supplied billet to the fully heat-treated disc, in order to establish the origin of the different η morphologies present in the final component.

3. Experimental methods

3.1. Materials

The 718Plus material used in this study was supplied by Rolls-Royce Deutschland Ltd. & Co KG (RRD). The alloy was triple vacuum melted for a premium quality ingot, and the precise chemical composition is presented in Table 1. The forging and heat treatment processes have been developed by RRD in collaboration with Otto Fuchs KG within the German-funded framework LuFoIV.

The three material conditions examined are:

i. Wrought billet, as provided by ATI Allvac (Allegheny Technologies Incorporated Allvac, Monroe, NC, USA).
ii. As-forged disc, produced from the billet material by several sub-solvus hot working operations.
iii. Fully heat-treated disc, subject to the standard heat treatment recommended by ATI Allvac [19]:
   - Pre-solution: 843 °C–871 °C / 16 h / AC
   - Solution: 954 °C–982 °C / 1 h / AC
   - Aging: 788 °C / 2 h – 8 h / FC + 704 °C / 8 h / AC.

3.2. Scanning electron microscopy

For imaging and quantitative analysis of the η-phase, the specimens were electro-etched in a solution 10 vol.% phosphoric acid in distilled water at 2.5 V to reveal the η and γ' precipitates. Secondary electrons (SE) were used to image the specimens in a scanning electron microscope (SEM) Jeol 5800LV, at a working distance of 10 mm and an acceleration voltage of 20 kV.

The micrographs were subsequently processed for image analysis using the software ImageJ [21]. To measure the area fraction of η-phase, the greyscale images were converted to binary maps by manually adjusting the threshold. This technique generally overestimated the precipitate content due to the metallographic preparation method, but gave information on the relative trends between samples. Ellipse fitting of the particle binary masks was used to determine plate alignment and aspect ratio.

A field emission gun SEM CamScan MX2600 was used for electron back-scatter diffraction (EBSD) mapping, with an accelerating voltage of 25 kV, sample tilt of 70° and working distance of 30 mm. The samples were polished to 0.06 μm colloidal silica finish and the results were analysed using HKL Channel5 software [22].

3.3. Transmission electron microscopy

Transmission electron microscopy (TEM) specimens were produced from 3 mm diameter discs. The discs were spark-eroded from slices 0.2–0.3 mm thick and then twin-jet electropolished with a solution 10 vol.% perchloric acid in methanol at −5 °C and 20.5 V. A Jeol 200CX microscope was used to examine the samples in the bright field and obtain electron diffraction patterns at an accelerating voltage of 200 kV.

4. Results

4.1. SEM imaging

4.1.1. Billet material

The microstructure of 718Plus wrought billet in the as-received condition was examined as the starting stock for the manufacture of a disc rotor. Since heating times for industrial-scale forging operations range from 30 min to 3 hours, the effect of hold time below the η-phase solvus has been studied through several short-term annealing heat treatments at temperatures between 925 °C and 1000 °C, and times 20 minutes, 1 hour and 3 hours.

The grain size in the as-received billet ranges from an average ASTM 8 in the centre to ASTM 12 close to the surface. The volume fraction and morphology of η-phase after hold time also varies along the cross-section, mainly due to differences in residual strain in the matrix from the ingot-to-billet conversion operation. A representative image of the η-structure after annealing for 3 hours at 950 °C, illustrative of heating time prior to sub-solvus forging, is shown in Fig. 2. The amount of η-phase present is as high as 4.4% in the billet centre and 8.5% in the billet surface. The complete results of this study will be reported elsewhere.

4.1.2. As-forged disc

Cube-shaped specimens were extracted from five different locations throughout the forging: three of them near

Table 1. Chemical composition of the ATI 718Plus material used in this study in wt.%. Balance is wt.%.

	Cr	Fe	Co	Nb	Mo	Al	Ti	W	C	P	B
718Plus	17.97	9.64	9.09	5.49	2.69	1.6	0.75	1.02	0.022	0.009	0.005

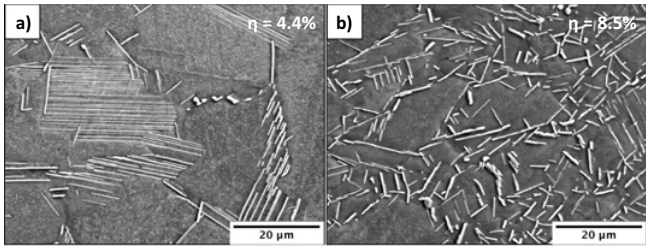

Figure 2. η-phase precipitation throughout the cross-section of 718Plus wrought billet: a) billet centre and b) billet surface.

the surface and two in the bulk. SEM specimens were subsequently cut along three different planes: axial-radial (AR), axial-tangential (AT) and tangential-radial (TR). Figure3 shows representative microstructures of the surface and bulk areas within the as-forged disc.

In both locations the morphology of the precipitates is that of relatively coarse platelets, which appear to be aligned along the TR plane, as confirmed by the three orientations examined. The η-phase content is high in the surface of the forging, between 9 and 10% along the AR and AT orientations. In the TR orientation that value is around 6%, noticeably lower although still very significant. The bulk, on the other hand, presents much lower amounts of precipitation in all orientations, between 1 and 2.5%. The lower η-phase content in the TR orientation for both locations could be explained by the alignment of the plates along that plane, as the metallographic preparation can easily have delaminated the precipitates parallel to the surface.

Due to heat transfer to the dies and higher cooling rates between hot working operations, the surface of the disc experiences temperature conditions below the nominal forging temperature; the precipitates present in the billet are therefore preserved. The opposite applies to the bulk, where adiabatic heating can locally induce temperature conditions over the η solvus. The low η-phase content can then be explained by the partial dissolution of any pre-existing precipitates. In summary, the different temperature conditions throughout the disc during deformation can result in a profoundly inhomogeneous as-forged microstructure.

The alignment is assumed to result from the rotation of pre-existing particles, which are unpinned from their nucleation sites and reoriented by the material flow and grain deformation during hot working. Signs of precipitate deformation and breakage are observed, as well as particles delimiting old grain boundaries and twins. A similar although less pronounced *forming-induced arrangement* has been reported for δ-phase in alloy 718 by Ponnelle *et al.* [23]. In γ–γ'–δ eutectic alloys, with high δ-phase contents up to 40 vol%, this effect can be more prominent [24].

4.1.3. Heat-treated disc

The same locations were investigated after heat treatment and representative micrographs are shown in Fig. 4. The precipitate content in the surface area, already significant after hot working, increased further to values up to 15%. The increase was more pronounced in the bulk: from the 2% in the as-forged state to well over 10% after heat treatment (see Fig. 5). Despite the extensive precipitation in the bulk during annealing, the overall η-phase content remained below that of the surface area.

Figure 6 illustrates the changes in the alignment and morphology of the precipitates after heat treatment. In the surface, the particles retained their plate-like shape and grew slightly coarser, which resulted in a similar orientation distribution. In the bulk, the pre-existing small and coarse plates appear combined with the new precipitation of long and thin lamellae growing in close-packed cascades with random orientations. As a result, the morphology distribution shifts to higher aspect ratios and, although the alignment of the thick plates is still evident, the overall particle orientation is randomised. The presence of thin lamellae is not exclusive to the bulk region and they can be observed to a lesser extent in the surface, where the predominant population is however formed by blocky plates aligned with the forging flow.

The results confirm that the typical η structure in the final component has a dual morphology: a combination of blocky aligned particles and thin lamellae in randomly oriented cascades. The different balances between the two populations found along the cross-section would respond to local variations in the temperature conditions during forging: in the bulk, most of the precipitation takes place during heat treatment, while the majority of precipitates in the surface zones were already present in the as-forged state. The particles that nucleate in the billet prior to forging are subsequently broken, unpinned from their original nucleation sites and aligned with the forging flow, all whilst the matrix recrystallises around them. As a result they must develop incoherent interfaces, which allow uniform coarsening during heat-treatment. The particles nucleated during annealing in fully recrystallised strain-free material, grow coherently with the matrix through a ledge-wise mechanism that promotes a fine lamellar morphology [16,25] .

4.2. TEM imaging

Bright-field TEM imaging of as-forged material provides evidence of dynamic recrystallisation during hot working (see Fig. 7). While the bulk appears to be fully recrystallised, in the surface region the recrystallised grains are surrounded by highly deformed areas in which sub-grain structures can be observed. The η precipitates present in the microstructure show signs of deformation and breakage, and often appear intragranularly, as well as at grain boundaries and triple points.

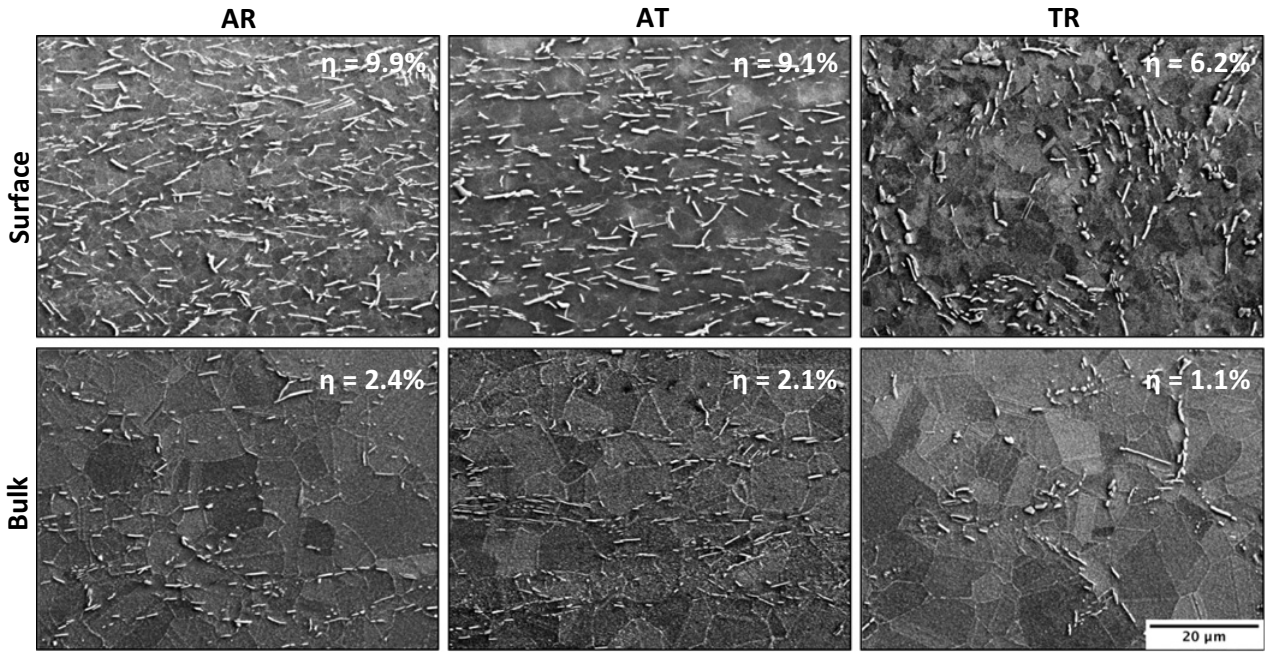

Figure 3. Microstructure and η-phase content in the as-forged condition in surface and bulk locations along three different orientations.

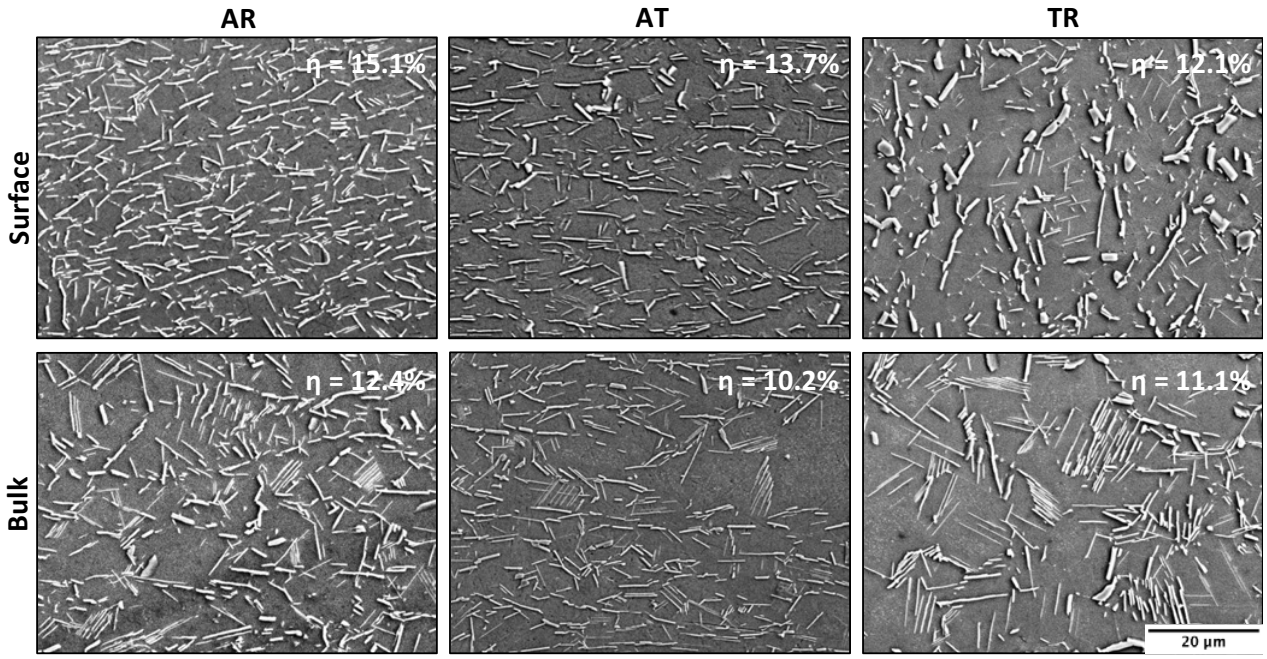

Figure 4. Microstructure and η-phase content in the heat-treated condition in surface and bulk locations along three orientations.

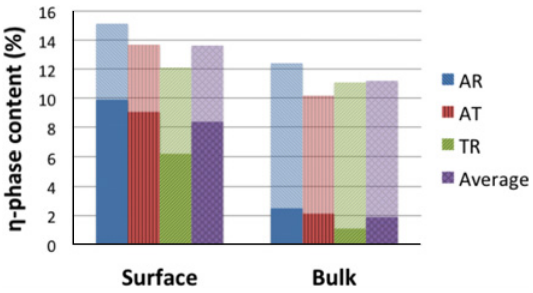

Figure 5. Measured η-phase area fraction in the as-forged (solid bars) and heat-treated (transparent bars) conditions.

As expected, imaging of the heat-treated material revealed a combination of plate-like particles with colonies of lamellae that seem to have an orientation relationship with the matrix. Selected-area electron diffraction patterns (SADPs) of those lamellae confirmed the Blackburn orientation relationship proposed by Pickering *et al.* [15], $\{11\bar{1}\}_\gamma \parallel (0001)_\eta$ and $\langle 1\bar{1}0\rangle_\gamma \parallel \langle 2\bar{1}\bar{1}0\rangle_\eta$, as shown in Fig. 8.

The coarse plate-like particles, on the other hand, do not satisfy any specific orientation relationship with the matrix, and their zone axes rarely match. Figure 9 shows an example of the SADP obtained from a blocky particle

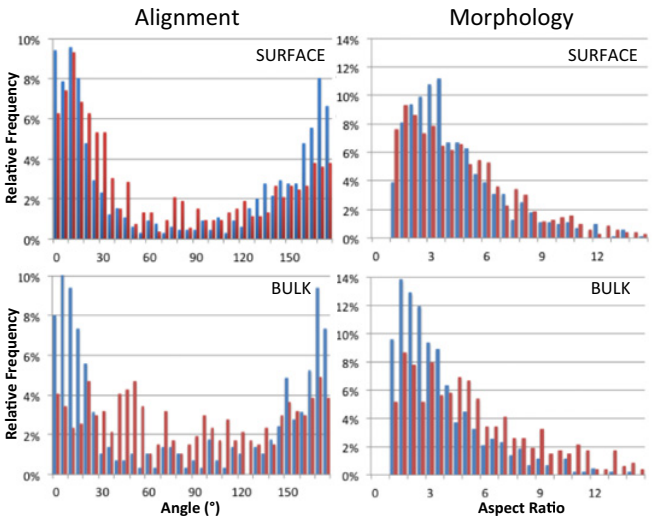

Figure 6. Alignment and aspect ratio of η precipitates in the AR orientation for as-forged (blue) and heat-treated (red) conditions.

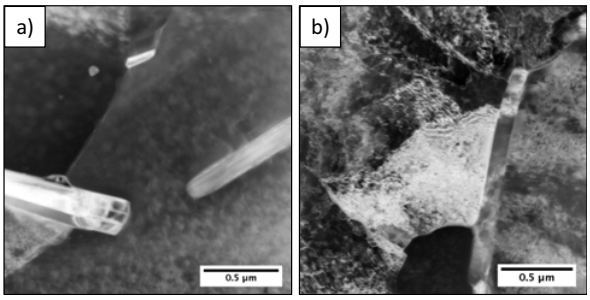

Figure 7. Bright field TEM micrographs of as-forged material from a) the disc bulk; and b) the disc surface.

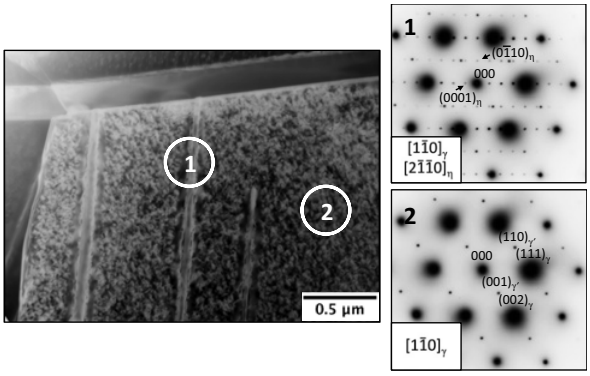

Figure 8. $[1\bar{1}0]_\gamma$ SADPs obtained from lamellar η precipitate in heat-treated material (1) and the adjacent γ/γ' region (2).

along the $[2\bar{1}\bar{1}0]_\eta$ zone axis. The pattern from the matrix, instead of the expected $[1\bar{1}0]_\gamma$, is indefinite.

4.3. EBSD analysis

EBSD was used to produce orientation maps of the η and γ phases in forged material from the surface area, which was annealed at 955 °C for 5 hours. This heat treatment was found to promote the coarsening of existing particles and

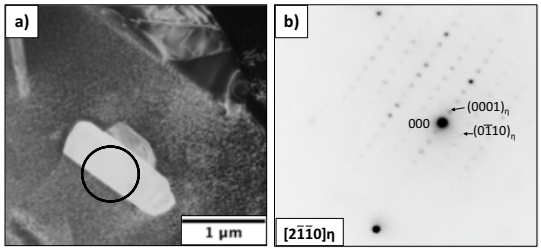

Figure 9. (a) Site of SADP in heat-treated material; (b) $[2\bar{1}\bar{1}0]_\eta$ pattern obtained from blocky η precipitate.

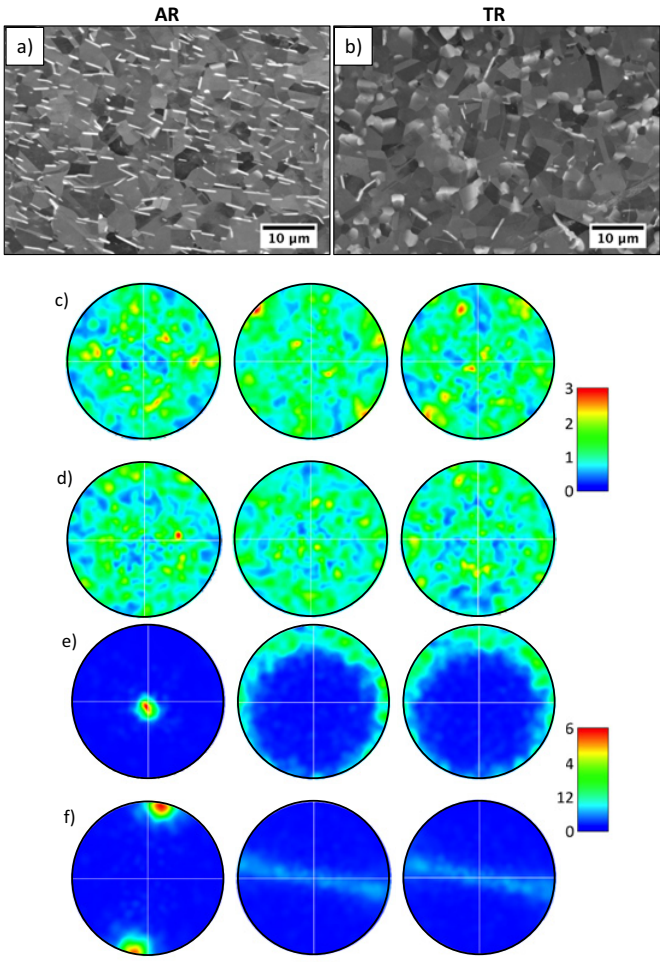

Figure 10. Pole figures calculated for the η and γ subsets: (a and b) microstructure of the areas mapped (back-scatter imaging and colloidal silica finish); (c and d) $(100)_\gamma$, $(110)_\gamma$ and $(111)_\gamma$ pole figures of γ-phase in the AR and TR orientations, respectively; (e and f) $(0001)_\eta$, $(11\bar{2}0)_\eta$ and $(10\bar{1}0)_\eta$ poles figures of η-phase in the AR and TR orientation, respectively.

improve indexation. The microstructure was mapped along two planes, AR and TR, over an area of $110 \times 85\ \mu m^2$ and with a $0.1\ \mu m$ step size. The pole figures are presented in Fig. 10 (note the differences in scale).

The η phase showed a marked texture where the $[0001]_\eta$ axis is strongly oriented with a 15° tilt with respect to the axial direction of the disc, matching the alignment observed in the microstructure (see Fig. 10a), while the

$[11\bar{2}0]_\eta$ axis is arbitrarily oriented along the perpendicular plane. The preferred crystallographic orientation of the η phase cannot be correlated to any texture of the surrounding γ phase. This supports the idea that the precipitates are detached and re-arranged by the hot working flow during deformation, with independence of the γ grains that recrystallise around them.

5. Conclusions

The microstructure of 718Plus components after sub-solvus forging and heat treatment shows a dual population of η particles formed by a combination of coarse plates and cascades of thin lamellae. In order to assess the effect of each manufacturing operation on the η-structure, and determine the origin of the two morphologies, the microstructure evolution of the alloy was investigated at various stages of the processing route.

The results showed that the precipitates present in the billet material prior to forging are deformed and unpinned from their original nucleation sites during sub-solvus hot working. They consequently develop an incoherent interface with the matrix that provides increased mobility. The particles then grow uniformly through the subsequent processing operations and acquire a coarse-plate morphology. Additionally, this population appears strongly aligned with the local forging flow. On the other hand, the precipitates that form during the heat treatment in recrystallised strain-free material grow coherently into the matrix through a ledge-wise mechanism that promotes a fine lamellar morphology. The colonies of lamellae grow in close-packed random orientations that fulfil the Blackburn relationship with the host γ grains.

The uneven temperature and strain conditions throughout the cross-section of the disc during hot working result in different ratios of the two populations. The balance between both morphologies in the final microstructure can be achieved by controlling precipitation and dissolution processes during hot working. In alloy 718, forming-induced arrangements have been reported to improve dwell crack propagation rates in certain directions [23], and it has been suggested that plate orientation can be equally important in 718Plus [3]. Adjusting the fraction of aligned particles can therefore play a key role in improving specific mechanical properties.

This work is related to a comprehensive research programme on alloy ATI 718Plus conducted at Rolls-Royce Deutschland Ltd. & Co KG and funded by the German Bundesministerium für Wirtschaft und Technologie (BMWi) under grant number 20T0813. The financial support from Rolls-Royce plc and the UK Engineering and Physical Sciences Research Council (EPSRC) under EP/H022309/1 and EP/H500375/1 is also gratefully acknowledged. A. Casanova wishes to further extend her thanks to the Fundación Caja Madrid Trust for their sponsorship.

References

[1] R. Kennedy, *Superalloys 718 625 706 and Various Derivatives*, 1–14 (2005)
[2] R. Kennedy, W. D. Cao, T. Bayha, *International Symposium on Niobium for High Temperature Applications* (2003)
[3] M. Springmann, W. Rothkegel, D. Huenert, H. Schlums, *7th International Conference on Low Cycle Fatigue* (2013)
[4] E. a. Ott, J. Groh, H. Sizek, *Superalloys 718 625 706 and Various Derivatives*, 35–45 (2005)
[5] S. Oppenheimer, E. McDevitt, W. D. Cao, *Superalloys 718 625 706 and Various Derivatives*, 321–330 (2010)
[6] W. D. Cao, *Superalloys 718 625 706 and Various Derivatives* (2005)
[7] R. Cozar, A. Pineau, Metall. Mater. Trans. B, **4** (1973)
[8] L. Viskari, K. Stiller, Ultramicroscopy, **111**, 652–8 (2011)
[9] K. Löhnert, F. Pyczak, *Superalloys 718 625 706 and Various Derivatives*, 877–891 (2010)
[10] W. D. Cao, R. Kennedy, *Superalloys*, **3**, 1–9 (2004)
[11] C. Stotter, Int. J. Mater. Res., **99**, 376–380 (2008)
[12] X. Xie, G. W. J. Dong, C. Xu, W. D. Cao, R. Kennedy, *Superalloys 718 625 706 and Various Derivatives*, 179–191 (2005)
[13] X. Xie, C. Xu, G. Wang, J. Dong, W. D. Cao, R. Kennedy, Mater. Res., 193–202 (2005)
[14] X. Xie, J. Dong, G. Wang, W. You, J. Du, C. Zhao, Z. Wang, T. Carneiro, *Superalloys 718 625 706 and Various Derivatives*, **3**, 287–298 (2005)
[15] E. Pickering, H. Mathur, A. Bhowmik *et al.*, Acta Mater., **60**, 2757-2769 (2012)
[16] O. Messé, J. Barnard, E. Pickering, P. Midgley, C. Rae, Philos. Mag., **94**, 1132-52 (2014)
[17] K. Lhnert, Dissertation, Universitt Erlangen - Nürnberg, 2011
[18] E. T. McDevitt, S. M. Oppenheimer, R. M. Kearsey, J. Tsang, Mater. Sci. Forum, **706–709**, 2428–2433 (2012)
[19] W. D. Cao, R. Kennedy, *Allvac Technical Report*, (2006)
[20] C. T. Sims, N. S. Stoloff, W. C. Hagel, *Superalloys II*. New York: John Wiley & Sons, 1987
[21] W. Rasband, "ImageJ", v1.44o, National Institutes of Health, USA
[22] Oxford Instruments, "HKL Channel 5", v5.0.9.0
[23] S. Ponnelle, B. Brethes, A. Pineau, *Superalloys 718 625 706 and Various Derivatives*, **92**, 1–10 (2001)
[24] M. Detrois, R. Helmink, S. Tin, Mater. Sci. Eng. A, **586**, 236–244 (2013)
[25] G. J. Shiflet, M. A. Mangan, W. G. Meng, Interface Sci., **154**, 133–154 (1998)